Photon information efficient communication through atmospheric turbulence

Citation: Chandrasekaran, Nivedita, Jeffrey H. Shapiro, and Ligong Wang. "Photon Information Efficient Communication through Atmospheric Turbulence." Edited by Ronald E. Meyers, Yanhua Shih, and Keith S. Deacon. Quantum Communications and Quantum Imaging X (October 15, 2012).

As Published: http://dx.doi.org/10.1117/12.929832

Publisher: SPIE

Persistent URL: http://hdl.handle.net/1721.1/90849

Version: Author's final manuscript: final author's manuscript post peer review, without publisher's formatting or copy editing

Photon information efficient communication through atmospheric turbulence

Nivedita Chandrasekaran, Jeffrey H. Shapiro, and Ligong Wang

Massachusetts Institute of Technology, Research Laboratory of Electronics, Cambridge, MA 02139-4307, USA

ABSTRACT

High photon-efficiency (many bits/photon) optical communication is possible with pulse-position modulation and direct detection, and high spectral efficiency (many bits/sec-Hz) optical communication is possible with quadrature-amplitude modulation and coherent detection. These high efficiencies, however, cannot be achieved simultaneously unless multiple spatial modes are employed. Previous work for the vacuum-propagation channel has shown that achieving 10 bits/photon *and* 5 bits/sec-Hz is impossible with coherent detection, and it requires 189 low diffraction-loss spatial modes at the ultimate Holevo limit, and 4500 such modes at the Shannon limit for on-off keying with direct detection. For terrestrial propagation paths, however, the effects of atmospheric turbulence must be factored into the photon and spectral efficiency assessments. This paper accomplishes that goal by presenting upper and lower bounds on the turbulent channel's ergodic Holevo capacity for M-mode systems whose transmitters use either focused-beam, Hermite-Gaussian (HG), or Laguerre-Gaussian (LG) modes, and whose receivers do M-mode detection either with or without adaptive optics. The bounds show that use of adaptive optics will *not* be necessary for achieving high photon efficiency and high spectral efficiency through atmospheric turbulence, although receivers which do not use adaptive optics will need to cope with considerable crosstalk between the spatial patterns produced in their entrance pupils by the M-mode transmitter. The bounds also show the exact theoretical equivalence of the HG and LG mode sets for this application, generalizing a result previously established for the vacuum-propagation channel. Finally, our results show that the FB modes outperform the HG and LG modes in operation with and without adaptive optics.

Keywords: free-space optical communications, atmospheric turbulence, photon efficiency, spectral efficiency, Hermite-Gaussian modes, Laguerre-Gaussian modes

1. INTRODUCTION

Photon-starved optical communication links, such as the Lunar Laser Communications Demonstration,[1] place a premium on achieving high photon information efficiency (PIE), i.e., many bits/detected photon. Such performance can be realized with a pulse-position modulation (PPM) transmitter, and a direct-detection receiver.[2] On the other hand, future developments in fiber-optic communication are increasingly focused on achieving high spectral efficiency (SE), that is, many bits/sec-Hz.[3] This goal can be realized by employing a high-order quadrature-amplitude modulation (QAM) transmitter and a coherent-detection receiver.[4] Should *both* high photon efficiency *and* high spectral efficiency be desired, however, the preceding approaches fail: PPM achieves its high photon efficiency via bandwidth expansion, in which case its spectral efficiency is necessarily low; and coherent detection is fundamentally incapable of high photon efficiency, with heterodyne and homodyne detection's photon efficiencies, as determined from their classical (Shannon-limit) capacities, being bounded above by 1.44 bits/detected-photon and 2.89 bits/detected-photon, respectively.[5]

Recourse to the ultimate quantum-mechanical (Holevo-limit) capacity of the bosonic (optical communication) channel does *not* eliminate the conflicting demands of high photon efficiency and high spectral efficiency. Consider the vacuum-propagation channel, in which the only noise injected is the minimum (vacuum-state) quantum noise needed to preserve the Heisenberg uncertainty principle. Here the photon information efficiency and the spectral efficiency for single spatial-mode operation, found from the Holevo-limit capacity,[6] are

$$\mathrm{PIE}_1 = [(1+\eta N_T)\log_2(1+\eta N_T) - \eta N_T \log_2(\eta N_T)]/\eta N_T, \tag{1}$$

Further author information: Send correspondence to N.C. at nivedita@mit.edu.

Quantum Communications and Quantum Imaging X, edited by Ronald E. Meyers, Yanhua Shih, Keith S. Deacon, Proc. of SPIE Vol. 8518, 851808 · © 2012 SPIE
CCC code: 0277-786/12/$18 · doi: 10.1117/12.929832

and

$$\mathrm{SE}_1 = (1+\eta N_T)\log_2(1+\eta N_T) - \eta N_T \log_2(\eta N_T), \tag{2}$$

where N_T is the average number of transmitted photons and η is the channel transmissivity, namely the fraction of the transmitted photons that are detected. Figure 1(a) shows the Holevo-limit PIE_1 versus SE_1 behavior, together with the corresponding Shannon-limit results for heterodyne and homodyne detection: none of them realizes both high photon information efficiency and high spectral efficiency.

High PIE and high SE *can* be realized together if we go to multiple spatial-mode operation, for which we have the Holevo-limit results[5]

$$\mathrm{PIE}_M = M[(1+\eta N_T/M)\log_2(1+\eta N_T/M) - (\eta N_T/M)\log_2(\eta N_T/M)]/\eta N_T, \tag{3}$$

and

$$\mathrm{SE}_M = M[(1+\eta N_T/M)\log_2(1+\eta N_T/M) - (\eta N_T/M)\log_2(\eta N_T/M)], \tag{4}$$

for M-mode operation over the vacuum-propagation channel when all M modes have the same transmissivity. Unfortunately, no explicit approach to realizing this capacity is known as yet. Moreover, as seen in Fig. 1(b), heterodyne and homodyne detection have hard limits—1.44 and 2.89 bits/detected-photon, respectively—on their PIE_M values. On the other hand, Fig. 1(b) also shows that the Shannon capacity of direct detection with on-off keying (OOK) mimics the 189 spatial-mode Holevo capacity, *but* to do so it requires 4500 equal-transmissivity spatial modes.[5] Bridging this large gap between the mode-number required by a known implementation for realizing both high PIE and high SE and the corresponding requirement at the ultimate quantum limit is the subject of ongoing research.[7,8]

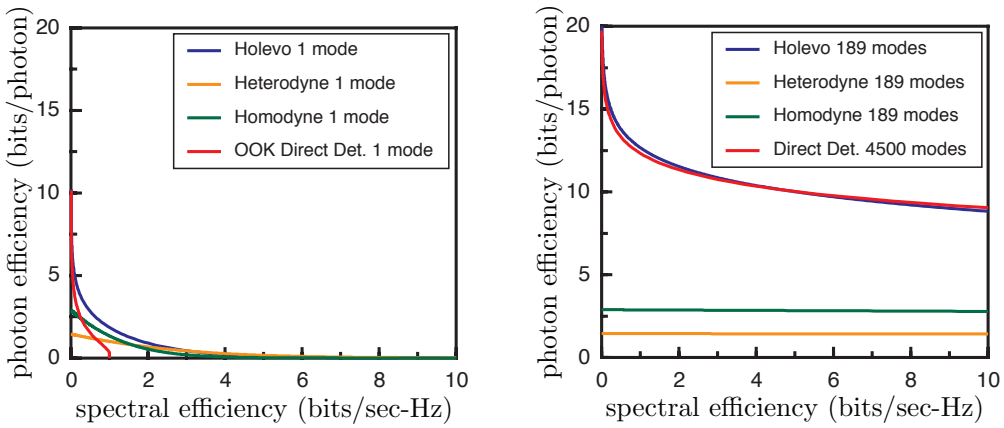

(a) Single spatial-mode operation (b) Multiple spatial-mode operation

Figure 1: Photon efficiency versus spectral efficiency for single spatial-mode and multiple spatial-mode vacuum-propagation links. Results for systems that achieve the Holevo capacity, the Shannon capacities of heterodyne detection and homodyne detection, and the Shannon capacity of direct detection with OOK modulation are shown.

Well-known propagation characteristics[9] of the vacuum-propagation channel imply that high photon efficiency with high spectral efficiency can only be obtained in the near-field power transfer regime. For an L-m-long line-of-sight vacuum-propagation link at wavelength λ between coaxial square transmitter and receiver pupils with sides of length d_T and d_R, respectively, near-field power transfer prevails when the Fresnel number product $D_f = (d_T d_R/\lambda L)^2$ satisfies $D_f \gg 1$.* Under this condition, there are approximately D_f orthonormal spatial

*Although circular pupils are more common, the square-pupil case is more convenient for the numerical evaluations that will be performed later. The physics of near-field propagation with coaxial circular pupils is the same as stated here for square pupils, except that the Fresnel number product is given by $D_f = (\pi D_T D_R/4\lambda L)^2$ in terms of the pupil diameters, D_T and D_R.

modes in the transmitter pupil—for each of two orthogonal polarization states—that transfer almost all of their power *and* retain their orthogonality after propagation into the receiver pupil. It follows that achieving the goal of operating at 10 bits/photon with 5 bits/sec-Hz will only be practical for very modest path lengths. For example, when $d_T = d_R = d$ and $\lambda = 1.55\,\mu$m, $D_f = 189$ (the Holevo limit) requires that $d = 15\,$cm when $L = 1\,$km. When $L = 10\,$km, the Holevo limit requires that $d = 46\,$cm. Switching to OOK direct detection, under the same pupil and wavelength assumptions, we find that $D_f = 4500$ requires that $d = 32\,$cm when $L = 1\,$km and $d = 1.0\,$m when $L = 10\,$km.

Application scenarios for these short path lengths will almost certainly involve terrestrial, rather than vacuum-propagation, paths. As such, they will be subject to the usual issues in short-range free-space optical communications.[†10,11] It has long been known that the presence of clouds or fog along the line of sight prevents high data-rate (Gbps) free-space optical communication.[12] So, if we are interested in high data-rate transmission with high photon and spectral efficiencies, only clear-weather propagation can be considered. Putting aside the modest extinction loss associated with atmospheric absorption and scattering at a well-chosen laser wavelength, it is the parts per million refractive-index fluctuations associated with turbulent mixing of air parcels with $\sim$1 K temperature differences—which lead to beam spread, angle-of-arrival spread, and time-dependent fading known as scintillation[13]—that distinguish clear-weather atmospheric propagation from propagation through vacuum. Thus the main task of this paper will be to establish bounds on the PIE versus SE behavior that can be realized using multiple spatial modes in the presence of atmospheric turbulence.

A great deal is known about wave propagation and optical communication through atmospheric turbulence, but only a limited amount of that work is germane to determining the degree to which this channel permits high PIE and high SE to be achieved simultaneously. We know that the atmospheric channel has a near-field power transfer regime—although with stochastic mode functions and modal transmissivities—that is similar to that of vacuum propagation.[14] Relatively little has been done, however, to assess the communication performance obtainable in this regime, with the exception of single spatial-mode studies of binary communication performance,[15] and single spatial-mode operation of the Bennett-Brassard 1984 (BB84) protocol for quantum key distribution.[16] This lack of results is due, in part, to the difficulty of determining the statistics of the turbulent channel's near-field modal transmissivities. Hence our capacity results will be built on the limited transmissivity-statistics that can be gleaned from existing propagation theory.

The rest of the paper is organized as follows. Section 2 provides a quick summary of the near-field modal decomposition of the turbulent channel specialized to M spatial-mode optical communication systems that use or do not use adaptive optics. Section 3 builds on this foundation by establishing upper and lower bounds on the turbulent channel's ergodic Holevo capacity that can be evaluated from the statistics provided in Section 2. Section 4 instantiates the bounds from Section 3 for three specific mode sets: focused-beam modes, Hermite-Gaussian (HG) modes, and Laguerre-Gaussian (LG) modes. Here it is found that adaptive optics will *not* be necessary for achieving high photon efficiency and high spectral efficiency through atmospheric turbulence, although receivers which do not use adaptive optics will need to cope with considerable crosstalk between the spatial patterns produced in their entrance pupils by the M-mode transmitter. It will also be seen that there is an exact theoretical performance equivalence between the HG and LG mode sets. These results make choosing between the HG and LG mode sets a matter of implementation convenience, which generalizes a result previously found for the vacuum-propagation channel.[17] In addition, we will find that that the FB modes outperform the HG and LG modes in operation with and without adaptive optics. Section 5 concludes with a summary of our results and areas for future study.

2. NEAR-FIELD MODAL DECOMPOSITION AND ITS STATISTICS

Consider propagation through atmospheric turbulence of linearly-polarized, quasimonochromatic light with center wavelength λ from a $d_T \times d_T$ transmitter pupil $\mathcal{A}_T$ in the $z = 0$ plane to a $d_R \times d_R$ receiver pupil $\mathcal{A}_R$ in the $z = L$ plane, as shown in Fig. 2. From the extended Huygens-Fresnel principle[13] we have that the complex

[†]Calling a line-of-sight optical link through the atmosphere a "free-space" link is common usage, which we will employ, although it is a misnomer. We reserve the term vacuum propagation for propagation through what electromagnetic theory would consider to be free space.

envelope, $E_L(\boldsymbol{\rho}', t)$, in the receiver's entrance pupil is related to the complex envelope in the transmitter's exit pupil, $E_0(\boldsymbol{\rho}, t)$, by the superposition integral[‡]

$$E_L(\boldsymbol{\rho}', t) = \int_{\mathcal{A}_T} d\boldsymbol{\rho}\, E_0(\boldsymbol{\rho}, t - L/c) h(\boldsymbol{\rho}', \boldsymbol{\rho}, t), \text{ for } \boldsymbol{\rho}' \in \mathcal{A}_R, \tag{5}$$

where $h(\boldsymbol{\rho}', \boldsymbol{\rho}, t)$ is the atmospheric Green's function at time t, and we have exploited the fact that turbulence-induced multipath spread is sub-ps and that Gbps communication can be accomplished with ns-duration pulses in assuming that the temporal behavior is just the line-of-sight propagation delay L/c. Furthermore, because the coherence time of the turbulence is ∼ms, we can safely limit our attention, in all that follows, to a single atmospheric state and suppress the Green's function's time argument.

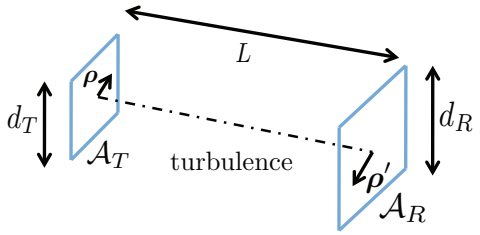

Figure 2: Atmospheric-channel propagation geometry.

The normal-mode decomposition associated with Eq. (5) provides power-transfer eigenvalues (modal transmissivities) that determine the achievable photon information efficiency and spectral efficiency of this channel state when both the transmitter and the receiver have and use knowledge of that state's Green's function $h(\boldsymbol{\rho}', \boldsymbol{\rho})$. We will be concerned, however, with the more restrictive—and more practical—case of multi-spatial-mode transmitters that employ fixed sets of M spatial modes, and receivers that extract M spatial modes either with or without the use of adaptive optics. The statistics of the power-transfer eigenvalues for these M-mode configurations then determine the ergodic Holevo capacities for operation with or without adaptive optics, and so establish the degree to which the performance shown in Fig. 1(b) is affected by the presence of turbulence. Because the statistics of these near-field power-transfer eigenvalues are not available analytically, we shall use the well-known mutual coherence function for $h(\boldsymbol{\rho}', \boldsymbol{\rho})$ to obtain eigenspectra that are majorized by the average power-transfer eigenvalues. Section 3 will then demonstrate how these eigenspectra lead to lower bounds on the ergodic capacities of systems that do or do not use adaptive optics. So, in preparation for developing those bounds, the subsections that follow will: review the normal-mode decomposition associated with Eq. (5); develop corresponding mode decompositions for M spatial-mode systems with or without adaptive optics; and use the Green's function's mutual coherence function to obtain modal power-transfer statistics that will permit us to lower bound the ergodic capacities of interest.

2.1. Normal-Mode Decomposition of the Turbulent Channel

The normal-mode decomposition for a single atmospheric state—Eq. (5) with the Green's function's time dependence suppressed—consists of: (1) a complete, orthonormal (CON) set of input transverse modes $\{\, \Phi_m(\boldsymbol{\rho}) : 1 \le m < \infty, \boldsymbol{\rho} \in \mathcal{A}_T \,\}$, (2) a CON set of transverse output modes $\{\, \phi_m(\boldsymbol{\rho}') : 1 \le m < \infty, \boldsymbol{\rho}' \in \mathcal{A}_R \,\}$, and (3) a set of power-transfer eigenvalues $\{\, \eta_m : 1 \le m < \infty \,\}$ such that

$$\int_{\mathcal{A}_T} d\boldsymbol{\rho}\, h(\boldsymbol{\rho}', \boldsymbol{\rho}) \Phi_m(\boldsymbol{\rho}) = \sqrt{\eta_m}\, \phi_m(\boldsymbol{\rho}'), \text{ for } \boldsymbol{\rho}' \in \mathcal{A}_R \text{ and } 1 \le m < \infty. \tag{6}$$

Physically, Eq. (6) states that transmission of $\Phi_m(\boldsymbol{\rho})$ from $\mathcal{A}_T$ results in reception of $\sqrt{\eta_m}\, \phi_m(\boldsymbol{\rho}')$ in $\mathcal{A}_R$. Because the input and output modes are normalized, it follows that η_m is the fractional power-transfer from $\mathcal{A}_T$ to $\mathcal{A}_R$ that is achieved when $\Phi_m(\boldsymbol{\rho})$ is transmitted. Without loss of generality we will assume that the modes are

[‡]No loss of generality is incurred by employing a scalar-wave theory, because turbulence does not cause depolarization.[18]

ordered so that the modal transmissivities are nonincreasing, i.e., $1 \geq \eta_1 \geq \eta_2 \geq \cdots \eta_m \geq \cdots \geq 0$, where the upper limit follows from the passive nature of propagation through turbulence.

When $h(\boldsymbol{\rho}', \boldsymbol{\rho})$ is known, the input modes, output modes, and eigenvalues can be found as follows. First solve the Fredholm equation[19, 20]

$$\int_{\mathcal{A}_T} d\boldsymbol{\rho}_2 \, K(\boldsymbol{\rho}_1, \boldsymbol{\rho}_2) \Phi_m(\boldsymbol{\rho}_2) = \eta_m \Phi_m(\boldsymbol{\rho}_1), \text{ for } \boldsymbol{\rho}_1 \in \mathcal{A}_T, \tag{7}$$

where

$$K(\boldsymbol{\rho}_1, \boldsymbol{\rho}_2) = \int_{\mathcal{A}_R} d\boldsymbol{\rho}' \, h^*(\boldsymbol{\rho}', \boldsymbol{\rho}_1) h(\boldsymbol{\rho}', \boldsymbol{\rho}_2), \tag{8}$$

to obtain the input modes and the eigenvalues, and then use Eq. (6) to get the output modes.

For vacuum propagation, when $h(\boldsymbol{\rho}', \boldsymbol{\rho})$ reduces to the Fresnel-diffraction Green's function,

$$h_L(\boldsymbol{\rho}' - \boldsymbol{\rho}) = \frac{\exp[ik(L + |\boldsymbol{\rho}' - \boldsymbol{\rho}|^2/2L)]}{i\lambda L}, \tag{9}$$

with $k = 2\pi/\lambda$, normal-mode decompositions are available for both square-pupil and circular-pupil geometries.[9, 21] These have the near-field power-transfer characteristics described in Section 1, when their respective Fresnel number products satisfy $D_f \gg 1$. For propagation through turbulence, however, the input modes, output modes, and eigenvalues are, in general, random. Nevertheless, the eigenvalues satisfy

$$\sum_{m=1}^{\infty} \eta_m = \int_{\mathcal{A}_R} d\boldsymbol{\rho}' \int_{\mathcal{A}_T} d\boldsymbol{\rho} \, |h(\boldsymbol{\rho}', \boldsymbol{\rho})|^2, \tag{10}$$

from which is has been shown[14] that the ensemble average of this sum equals the vacuum-propagation Fresnel number product, and that similar near-field power transfer behavior prevails for the turbulent atmosphere as previously described for vacuum propagation, viz., when $D_f \gg 1$ there are $\sim D_f$ input modes whose associated power-transfer eigenvalues are near unity.

2.2. M Spatial-Mode Links with and without Adaptive Optics

The best high-PIE, high-SE communication performance through atmospheric turbulence would result from near-field operation with a transmitter that tracked and employed the M input spatial modes for each atmospheric state whose power-transfer eigenvalues were the highest. Implementing such a system, however, would be quite demanding. So we will consider a simpler transmitter that uses a fixed set of M orthonormal input modes

$$\boldsymbol{\Phi}^{(0)}(\boldsymbol{\rho}) = \left[\begin{array}{cccc} \Phi_1^{(0)}(\boldsymbol{\rho}) & \Phi_2^{(0)}(\boldsymbol{\rho}) & \cdots & \Phi_M^{(0)}(\boldsymbol{\rho}) \end{array} \right]^T, \text{ for } \boldsymbol{\rho} \in \mathcal{A}_T, \tag{11}$$

where ^{T} denotes transpose, and the superscripts are meant to distinguish this fixed mode set from the atmosphere's instantaneous input modes, $\{\Phi_m(\boldsymbol{\rho})\}$, introduced in the previous subsection. We will choose specific $\boldsymbol{\Phi}^{(0)}(\boldsymbol{\rho})$ in Section 4. For now, it suffices to say that these will be mode sets that approximate the vacuum-propagation input modes—for the same propagation geometry—with the highest associated power transfers and arranged in nonincreasing power-transfer order.

The transmitter encodes and sends information to the receiver via the $z = 0$ plane complex envelope

$$E_0(\boldsymbol{\rho}, t) = \sum_{m=1}^{M} E_{\text{in}_m}(t) \Phi_m^{(0)}(\boldsymbol{\rho}) = \boldsymbol{\Phi}^{(0)T}(\boldsymbol{\rho}) \mathbf{E}_{\text{in}}(t) \tag{12}$$

where

$$\mathbf{E}_{\text{in}}(t) = \left[\begin{array}{cccc} E_{\text{in}_1}(t) & E_{\text{in}_2}(t) & \cdots & E_{\text{in}_M}(t) \end{array} \right]^T, \tag{13}$$

is the set of temporal waveforms applied to the M spatial modes. Transmission of the spatial mode $\Phi_m^{(0)}(\boldsymbol{\rho})$ from the transmitter pupil $\mathcal{A}_T$ gives rise to reception of the spatial pattern

$$\zeta_m(\boldsymbol{\rho}') = \int_{\mathcal{A}_T} d\boldsymbol{\rho}\, h(\boldsymbol{\rho}', \boldsymbol{\rho}) \Phi_m^{(0)}(\boldsymbol{\rho}), \tag{14}$$

for $\boldsymbol{\rho}'$ in the receiver pupil $\mathcal{A}_R$. The collection of these M spatial patterns is, in general, random, owing to the random nature of the turbulent channel's Green's function. We will consider two possible receivers for extracting the information embedded in the received field,

$$E_L(\boldsymbol{\rho}', t) = \sum_{m=1}^{M} E_{\mathrm{in}_m}(t - L/c)\zeta_m(\boldsymbol{\rho}'). \tag{15}$$

The first uses ideal (full-wave) adaptive optics to extract M orthonormal modes from the vector space of spatial patterns spanned by $\{\, \zeta_m(\boldsymbol{\rho}') : 1 \le m \le M, \boldsymbol{\rho}' \in \mathcal{A}_R, \}$. The second extracts a fixed set of orthonormal modes

$$\boldsymbol{\phi}^{(0)}(\boldsymbol{\rho}') = \left[\; \phi_1^{(0)}(\boldsymbol{\rho}') \quad \phi_2^{(0)}(\boldsymbol{\rho}') \quad \cdots \quad \phi_M^{(0)}(\boldsymbol{\rho}') \;\right]^T, \text{ for } \boldsymbol{\rho}' \in \mathcal{A}_R, \tag{16}$$

where the superscripts are meant to distinguish this fixed mode set from the atmosphere's instantaneous output modes, $\{\phi_m(\boldsymbol{\rho}')\}$.

For both of the preceding receivers we shall assume that the receiver *and* the transmitter know the resulting power-transfer behavior, and they use this information to achieve the ergodic Holevo capacities with and without adaptive optics. Those ergodic capacities depend on the power-transfer eigenvalues—for the chosen transmitter modes and receiver mode-extraction approach—that are obtained as follows. For the adaptive optics receiver, we define a channel function

$$\mathbf{H}_{\mathrm{ad}}(\boldsymbol{\rho}') = \left[\; \zeta_1(\boldsymbol{\rho}') \quad \zeta_2(\boldsymbol{\rho}') \quad \cdots \quad \zeta_M(\boldsymbol{\rho}') \;\right]^T, \tag{17}$$

so that the received field is given by

$$E_L(\boldsymbol{\rho}', t) = \mathbf{H}_{\mathrm{ad}}(\boldsymbol{\rho}')\mathbf{E}_{\mathrm{in}}(t - L/c). \tag{18}$$

The power-transfer eigenvalues, $\{\, \mu_m^{\mathrm{ad}} : 1 \le m \le M \,\}$, that determine the ergodic Holevo capacity for the adaptive optics system are therefore those of the $M \times M$ Hermitian matrix

$$\mathbf{K}_{\mathrm{ad}} = \int_{\mathcal{A}_R} d\boldsymbol{\rho}'\, \mathbf{H}_{\mathrm{ad}}^{\dagger}(\boldsymbol{\rho}')\mathbf{H}_{\mathrm{ad}}(\boldsymbol{\rho}'), \tag{19}$$

where † denotes conjugate transpose.

Turning now to the receiver that extracts the fixed mode set $\boldsymbol{\phi}^{(0)}(\boldsymbol{\rho}')$, we have that this receiver obtains

$$\mathbf{E}_{\mathrm{out}}(t) = \mathbf{H}_{\mathrm{non}}\mathbf{E}_{\mathrm{in}}(t - L/c), \tag{20}$$

after mode extraction, where the channel matrix $\mathbf{H}_{\mathrm{non}}$ has its nmth element, h_{nm}, given by

$$h_{nm} = \int_{\mathcal{A}_R} d\boldsymbol{\rho}'\, \phi_n^{(0)*}(\boldsymbol{\rho}')\zeta_m(\boldsymbol{\rho}'), \text{ for } 1 \le n, m \le M. \tag{21}$$

The power-transfer eigenvalues, $\{\, \mu_m^{\mathrm{non}} : 1 \le m \le M \,\}$, that determine the ergodic Holevo capacity for the system without adaptive optics are therefore those of the $M \times M$ Hermitian matrix

$$\mathbf{K}_{\mathrm{non}} = \mathbf{H}_{\mathrm{non}}^{\dagger}\mathbf{H}_{\mathrm{non}}. \tag{22}$$

In general, the eigenvalues for the adaptive and non-adaptive mode extraction cases will be random, just as is the case for the $\{\, \eta_m : 1 \le m < \infty \,\}$ discussed in Section 2.1. Before attempting to characterize the statistics

of the $\{\mu_m^{\rm ad}\}$ and the $\{\mu_m^{\rm non}\}$, which we will undertake in the next subsection, it is worth noting the following majorization results,

$$\sum_{m=1}^{K}\eta_m \geq \sum_{m=1}^{K}\mu_m^{\rm ad} \geq \sum_{m=1}^{K}\mu_m^{\rm non}, \text{ for } 1\leq K\leq M, \tag{23}$$

where each set of eigenvalues has been arranged in nonincreasing order. These results are immediate consequences of the increasing constraints on the input and output mode sets as one goes from the $\{\eta_m\}$ to the $\{\mu_m^{\rm ad}\}$ to the $\{\mu_m^{\rm non}\}$.

2.3. Eigenvalue Statistics from the Extended Huygens-Fresnel Principle

To evaluate the prospects for optical communication with high photon efficiency and high spectral efficiency over an L-m-long line-of-sight path through the turbulent atmosphere—using either of the M spatial-mode systems described in the preceding subsection—we need to find the statistics of their respective power-transfer eigenvalues in the near-field regime, wherein the Fresnel number product is much greater than unity. The usual formulation of the extended Huygens-Fresnel principle, when atmospheric extinction is omitted, takes the Green's function for a single atmospheric state to be

$$h(\boldsymbol{\rho}',\boldsymbol{\rho}) = h_L(\boldsymbol{\rho}'-\boldsymbol{\rho})\exp[\chi(\boldsymbol{\rho}',\boldsymbol{\rho})+i\phi(\boldsymbol{\rho}',\boldsymbol{\rho})], \tag{24}$$

where $h_L(\boldsymbol{\rho}'-\boldsymbol{\rho})$ is the Fresnel diffraction (vacuum propagation) Green's function from Eq. (9), and $\chi(\boldsymbol{\rho}',\boldsymbol{\rho})$ and $\phi(\boldsymbol{\rho}',\boldsymbol{\rho})$ are real-valued random processes that represent the random logamplitude and phase fluctuations imposed on the field received at $\boldsymbol{\rho}'$ in the $z=L$ plane from a point source located at $\boldsymbol{\rho}$ in the $z=0$ plane. Physically, $\chi(\boldsymbol{\rho}',\boldsymbol{\rho})$ gives rise to scintillation, while $\phi(\boldsymbol{\rho}',\boldsymbol{\rho})$ is responsible for the beam spread and angle-of-arrival spread produced by the turbulence.

A great deal is known about the statistics of propagation through turbulence,[13,22–24] but as yet very little is known about the near-field statistics of the $\{\eta_m\}$ from Section 2.1, and, to our knowledge, no one has considered the near-field behavior of our $\{\mu_m^{\rm ad}\}$ and $\{\mu_m^{\rm non}\}$. In Section 3, we shall derive lower bounds on the ergodic Holevo capacities for adaptive and non-adaptive operation that only require knowledge of the ensemble averages, $\{\langle\mu_m^{\rm ad}\rangle\}$ and $\{\langle\mu_m^{\rm non}\rangle\}$, for their evaluation. Unfortunately, obtaining even these simple statistics would require Monte Carlo simulation when propagation is in the near-field power transfer regime. Thus we will content ourselves, in the present subsection, with showing how to obtain simpler, but nonetheless useful, power-transfer statistics by focusing our attention on the ensemble-average matrices $\langle\mathbf{K}_{\rm ad}\rangle$ and $\langle\mathbf{K}_{\rm non}\rangle$.

The nmth elements of $\langle\mathbf{K}_{\rm ad}\rangle$ and $\langle\mathbf{K}_{\rm non}\rangle$ are given by

$$\langle\mathbf{K}_{\rm ad}\rangle_{nm} = \int_{\mathcal{A}_R}d\boldsymbol{\rho}'\int_{\mathcal{A}_T}d\boldsymbol{\rho}_1\int_{\mathcal{A}_T}d\boldsymbol{\rho}_2\;\Phi_n^{(0)*}(\boldsymbol{\rho}_1)\langle h^*(\boldsymbol{\rho}',\boldsymbol{\rho}_1)h(\boldsymbol{\rho}',\boldsymbol{\rho}_2)\rangle\Phi_m^{(0)}(\boldsymbol{\rho}_2), \tag{25}$$

and

$$\langle\mathbf{K}_{\rm non}\rangle_{nm} = \sum_{k=1}^{M}\int_{\mathcal{A}_R}d\boldsymbol{\rho}_1'\int_{\mathcal{A}_R}d\boldsymbol{\rho}_2'\int_{\mathcal{A}_T}d\boldsymbol{\rho}_1\int_{\mathcal{A}_T}d\boldsymbol{\rho}_2\;\phi_k^{(0)}(\boldsymbol{\rho}_1')\phi_k^{(0)*}(\boldsymbol{\rho}_2')\langle h^*(\boldsymbol{\rho}_1',\boldsymbol{\rho}_1)h(\boldsymbol{\rho}_2',\boldsymbol{\rho}_2)\rangle\Phi_n^{(0)*}(\boldsymbol{\rho}_1)\Phi_m^{(0)}(\boldsymbol{\rho}_2), \tag{26}$$

from which we see that the only turbulence statistic needed to evaluate these ensemble-averaged matrices is the Green's function's mutual coherence function. This mutual coherence function satisfies[13,22]

$$\langle h^*(\boldsymbol{\rho}_1',\boldsymbol{\rho}_1)h(\boldsymbol{\rho}_2',\boldsymbol{\rho}_2)\rangle = h_L^*(\boldsymbol{\rho}_1',\boldsymbol{\rho}_1)h_L(\boldsymbol{\rho}_2',\boldsymbol{\rho}_2)\exp[-D(\boldsymbol{\rho}_2'-\boldsymbol{\rho}_1',\boldsymbol{\rho}_2-\boldsymbol{\rho}_1)/2], \tag{27}$$

where

$$D(\Delta\boldsymbol{\rho}',\Delta\boldsymbol{\rho}) = 2.91k^2\int_0^L dz\,C_n^2(z)|\Delta\boldsymbol{\rho}'z/L+\Delta\boldsymbol{\rho}(1-z/L)|^{5/3}, \tag{28}$$

is the two-source, spherical-wave, wave structure function, and $C_n^2(z)$ is the turbulence strength profile along the path from the transmitter ($z=0$) to the receiver ($z=L$). The initial derivation of this mutual coherence

function employed the Rytov approximation, and hence its validity was limited to the weak-perturbation regime before the onset of saturated scintillation. Subsequent work—employing the small-angle approximation to the transport equation or the local method of smooth perturbations applied to the parabolic equation—has shown that Eqs. (27) and (28) are valid in the saturation regime as well.

We can numerically evaluate the elements of $\langle \mathbf{K}_{\rm ad} \rangle$ and $\langle \mathbf{K}_{\rm non} \rangle$, and then (again numerically) diagonalize them to obtain their respective eigenvalues, $\{ \gamma_m^{\rm ad} : 1 \leq m \leq M \}$ and $\{ \gamma_m^{\rm non} : 1 \leq m \leq M \}$, which we shall take to be in nonincreasing order. Because the ensemble-averaged eigenvalues of a random $M \times M$ Hermitian matrix majorize the deterministic eigenvalues of the ensemble average of that matrix, we have that

$$\sum_{m=1}^{K} \langle \mu_m^{\rm ad} \rangle \geq \sum_{m=1}^{K} \gamma_m^{\rm ad}, \text{ for } 1 \leq K \leq M, \tag{29}$$

and

$$\sum_{m=1}^{K} \langle \mu_m^{\rm non} \rangle \geq \sum_{m=1}^{K} \gamma_m^{\rm non}, \text{ for } 1 \leq K \leq M. \tag{30}$$

In the next section we show that these majorization relations allow us to lower bound the ergodic Holevo capacities of adaptive and non-adaptive operation using eigenvalue statistics that only depend on knowing the atmospheric Green's function's mutual coherence function. It turns out, however, that full numerical evaluation of $\langle \mathbf{K}_{\rm non} \rangle$ for the mode sets we will consider in Section 4 is quite time consuming, whereas obtaining $\langle \mathbf{K}_{\rm ad} \rangle$ is relatively straightforward. Thus Section 4 will report $\{\gamma_m^{\rm ad}\}$ results, but only the diagonal elements of $\langle \mathbf{K}_{\rm non} \rangle$, which, when they arranged in nonincreasing order, we will denote $\{ \kappa_m^{\rm non} : 1 \leq m \leq M \}$. Because the eigenvalues of an Hermitian matrix majorize its diagonal elements, we know that

$$\sum_{m=1}^{K} \gamma_m^{\rm non} \geq \sum_{m=1}^{K} \kappa_m^{\rm non}, \text{ for } 1 \leq K \leq M. \tag{31}$$

Using the $\{\kappa_m^{\rm non}\}$ to lower bound the non-adaptive system's ergodic Holevo capacity provides a weaker result than what we would obtain were we to find the $\{\gamma_m^{\rm non}\}$. In Section 3 we will explain how the maximum difference between the $\{\gamma_m^{\rm non}\}$-based and $\{\kappa_m^{\rm non}\}$-based capacity bounds can be quantified, if desired.

3. ERGODIC HOLEVO CAPACITIES OF THE TURBULENT CHANNEL

The Holevo capacity, in bits per channel use, of a deterministic, pure-loss (vacuum-noise injection) M spatial-mode optical channel whose transmitter is constrained to use at most N_T photons on average is known to be[6]

$$C = \max_{\mathbf{N}: \sum_{m=1}^{M} N_m = N_T} \sum_{m=1}^{M} g\left(\eta_m N_m\right), \tag{32}$$

where $\mathbf{N} = \left[\begin{array}{cccc} N_1 & N_2 & \cdots & N_M \end{array} \right]$ is the vector of average photon numbers used for the M modes, the $\{\eta_m\}$ are the modal transmissivities, and $g(x)$ is the von Neumann entropy of a thermal state with average photon number x, i.e.,

$$g(x) = (x+1)\log_2(x+1) - x\log_2(x). \tag{33}$$

We are interested in the ultimate performance limit of M spatial-mode communication through the turbulent channel when the transmitter and receiver have and use knowledge of the power-transfer behavior. Here the relevant quantity is the ergodic Holevo capacity,

$$C_{\rm erg} = \left\langle \max_{\mathbf{N}: \sum_{m=1}^{M} N_m = N_T} \sum_{m=1}^{M} g\left(\mu_m N_m\right) \right\rangle \tag{34}$$

where throughout this section $\mu_m = \mu_m^{\rm ad}$ or $\mu_m^{\rm non}$, depending on whether we are interested in the system that does or does not employ adaptive optics.

Our objective is to bound the behavior of the ergodic Holevo capacities for adaptive and non-adaptive operation, because full statistics of their respective power-transfer eigenvalues are not available. Upper bounds are easily obtained. Because the power-transfer eigenvalues are bounded above by unity, and because the ergodic Holevo capacity is monotonically increasing with increases in any or all of the eigenvalues, we have that

$$C_{\rm erg} \leq M g(N_T/M), \tag{35}$$

for both adaptive and non-adaptive operation. Equation (35) leads to PIE_M and SE_M expressions identical to the $\eta = 1$ versions of Eqs. (3) and (4), respectively. We do not, however, expect that these ergodic capacity upper bounds will be tight, particularly for the receiver that does not use adaptive optics, so we turn our attention now to the more difficult—and more interesting—task of deriving lower bounds on the ergodic Holevo capacities for adaptive and non-adaptive operation.

Because the average of a maximum cannot be exceeded by the maximum of an average, we have that

$$C_{\rm erg} \geq \max_{\mathbf{N}:\, \sum_{m=1}^{M} N_m = N_T} \sum_{m=1}^{M} \langle g\left(\mu_m N_m\right)\rangle\,. \tag{36}$$

Because $g(\mu_m N_m)$, for fixed N_m, is a concave function of $\mu_m \in [0,1]$ with $g(0) = 0$, it follows that $\langle g(\mu_m N_m)\rangle \geq \langle\mu_m\rangle g(N_m)$ when $\langle\mu_m\rangle$ is given. As a result, we get

$$C_{\rm erg} \geq \max_{\mathbf{N}:\, \sum_{m=1}^{M} N_m = N_T} \sum_{m=1}^{M} \langle\mu_m\rangle g(N_m). \tag{37}$$

At this point we employ the fact, established in Section 2, that the $\{\langle\mu_m\rangle\}$ majorize the $\{\gamma_m\}$, where the latter can be found (numerically) from the atmospheric Green's function's mutual coherence function.

Consider the tentative lower bound

$$C_{\rm erg} \geq \max_{\mathbf{N}:\, \sum_{m=1}^{M} N_m = N_T} \sum_{m=1}^{M} \gamma_m g(N_m). \tag{38}$$

To prove the correctness of this assertion it suffices to demonstrate that, for $\mathbf{N}$ achieving the maximum in (38),

$$\sum_{m=1}^{M} \left(\langle\mu_m\rangle - \gamma_m\right) g\left(N_m\right) \geq 0, \tag{39}$$

which is easily accomplished from majorization. Rearranging terms in (39) we can write

$$\begin{aligned}
\sum_{m=1}^{M} \left(\langle\mu_m\rangle - \gamma_m\right) g\left(N_m\right) \;=\; & \left[\sum_{m=1}^{M} \left(\langle\mu_m\rangle - \gamma_m\right)\right] g(N_M) \\
& + \left[\sum_{m=1}^{M-1} \left(\langle\mu_m\rangle - \gamma_m\right)\right] [g(N_{M-1}) - g(N_M)] \\
& + \cdots \\
& + \left[\sum_{m=1}^{M-k} \left(\langle\mu_m\rangle - \gamma_m\right)\right] [g(N_{M-k}) - g(N_{M-k+1})] \\
& + \cdots \\
& + (\langle\mu_1\rangle - \gamma_1)[g(N_1) - g(N_2)].
\end{aligned} \tag{40}$$

With this rearrangement, proving (39) is quite simple. We know that $g(x)$ is a monotonically increasing, non-negative function of its argument. Moreover, because both the $\{\langle\mu_m\rangle\}$ and the $\{\gamma_m\}$ are nonincreasing with

increasing m, Lagrange-multiplier optimization—see below—will demonstrate that the maximizing $\mathbf{N}$ choice in (38) will have nonincreasing $\{N_m\}$ with increasing m. Therefore, in (40), we have $g(N_M) \geq 0$ and $g(N_{M-k}) - g(N_{M-k+1}) \geq 0$ for $1 \leq k \leq M-1$. The inequality in (39) then follows immediately from the $\{\gamma_m\}$ being majorized by the $\{\langle \mu_m \rangle\}$, and so we obtain the lower bounds on the ergodic Holevo capacities for adaptive and non-adaptive operation that can be computed from available knowledge of the atmospheric Green's function's mutual coherence function. We, however, will further weaken our lower bound for the non-adaptive case—because of the tedious nature of computing all the elements of $\langle \mathbf{K}_{\rm non} \rangle$—and content ourselves with the bound

$$C_{\rm erg}^{\rm non} \geq \max_{\mathbf{N}: \sum_{m=1}^{M} N_m = N_T} \sum_{m=1}^{M} \kappa_m^{\rm non} g(N_m), \tag{41}$$

which can be proven by reprising the development of (41) with $\gamma_m^{\rm non}$ used in lieu of $\langle \mu_m \rangle$, and $\kappa_m^{\rm non}$ employed in place of γ_m.

Note that

$$D_f^{\rm non} \equiv \sum_{m=1}^{M} \kappa_m^{\rm non} = \sum_{m=1}^{M} \gamma_m^{\rm non}, \tag{42}$$

because the trace of a matrix equals the sum of its eigenvalues. Furthermore, the $\{\gamma_m^{\rm non}\}$ are majorized by the $\{\alpha_m\}$, given by

$$\alpha_m = \begin{cases} 1, & \text{for } 1 \leq m \leq \lceil D_f^{\rm non} \rceil \\ 0, & \text{for } \lceil D_f^{\rm non} \rceil + 1 \leq m \leq M, \end{cases} \tag{43}$$

where $\lceil D_f^{\rm non} \rceil$, the smallest integer that is larger than $D_f^{\rm non}$, has been assumed to be less than M. It follows that

$$\lceil D_f^{\rm non} \rceil g(N_T / \lceil D_f^{\rm non} \rceil) \geq \max_{\mathbf{N}: \sum_{m=1}^{M} N_m = N_T} \sum_{m=1}^{M} \gamma_m^{\rm non} g(N_m), \tag{44}$$

which permits us to bound—if desired—how much weaker our ergodic Holevo capacity bound has become for non-adaptive operation by relying on the $\{\kappa_m^{\rm non}\}$ instead of the $\{\gamma_m^{\rm non}\}$.

In Section 4 we shall evaluate our lower bounds for three sets of input modes: focused-beam modes, Hermite-Gaussian modes, and Laguerre-Gaussian modes. The optimizing photon-number distribution across the M modes, found from Lagrange-multiplier procedures, is

$$N_m = \frac{1}{\exp(\beta_{\rm ad}/\gamma_m^{\rm ad}) - 1}, \tag{45}$$

when adaptive optics are employed, and

$$N_m = \frac{1}{\exp(\beta_{\rm non}/\kappa_m^{\rm non}) - 1}, \tag{46}$$

when they are not. In these equations, $\beta_{\rm ad}$ and $\beta_{\rm non}$ are chosen so that $\sum_{m=1}^{M} N_m = N_T$.

4. POWER-TRANSFER EIGENSTRUCTURE AND ERGODIC CAPACITY BOUNDS

Sections 2 and 3 have prepared us to bound the ergodic Holevo capacities that are realized with a transmitter which uses a fixed set of M spatial modes and receivers that do or do not use adaptive optics. We will use those results in the present section to examine the degree to which the photon information efficiency versus spectral efficiency behavior that we exhibited—for vacuum propagation with equal modal transmissivities—in Fig. 1(b) is degraded by propagation through atmospheric turbulence. Three specific transmitter mode sets will be considered: focused-beam (FB) modes, Hermite-Gaussian (HG) modes, and Laguerre-Gaussian (LG) modes. FB-mode transmitters are relatively simple to implement, whereas more complicated equipment is required for HG and LG operation. We have previously shown that HG and LG modes give identical Holevo capacities

in vacuum-propagation conditions.[17] Recent work, however, has addressed the use of LG modes for optical communication through turbulence,[25–27] motivated by the hope that the orbital angular momentum (OAM) these modes carry will make them more resistant to turbulence-induced crosstalk than HG modes, which do not carry OAM. Thus it is of interest for us to revisit the LG versus HG question in that context.

For the three mode sets to be considered, we shall employ the square-pupil setup shown in Fig. 2, with $d_T = d_R = 17.6\,\text{cm}$, $L = 1\,\text{km}$, and $\lambda = 1.55\,\mu\text{m}$, so that the vacuum-propagation Fresnel number product is $D_f = 400$. We shall assume a uniform turbulence-strength profile along the path from $z = 0$ to $z = L$, with constant C_n^2 values of either $5 \times 10^{-15}\,\text{m}^{-2/3}$ (mild turbulence) or $5 \times 10^{-14}\,\text{m}^{-2/3}$ (moderate turbulence). To simplify the numerical calculations, we shall employ the square-law approximation to the spherical-wave, wave structure function from Eq. (28), viz.,

$$D(\Delta\boldsymbol{\rho}', \Delta\boldsymbol{\rho}) = \frac{|\Delta\boldsymbol{\rho}'|^2 + \Delta\boldsymbol{\rho}' \cdot \Delta\boldsymbol{\rho} + |\Delta\boldsymbol{\rho}|^2}{\rho_0^2}, \tag{47}$$

where

$$\rho_0 = (1.09k^2 C_n^2 L)^{-3/5} \tag{48}$$

is the spherical-wave coherence length. Also of interest is the weak-perturbation (Rytov theory) spherical-wave logamplitude variance,

$$\sigma_\chi^2 = 0.124k^{7/6} C_n^2 L^{11/6}. \tag{49}$$

Values of ρ_0 and σ_χ^2 for the parameter values we have assumed and given in Table 1. Because the transmit and receive pupils are appreciably larger than the turbulence coherence length for the case of moderate turbulence, we can expect that significant beam spread and angle-of-arrival spread will occur. Likewise, the spherical-wave logamplitude variance for that turbulence strength implies that there will be considerable scintillation in the moderate-turbulence case. Thus, to ward off some of the ill effects of these turbulence-induced degradations, we shall only employ $M \sim 200$ FB, HG, and LG transmitter modes in our calculations, choosing those that achieve the best power transfers under vacuum-propagation conditions.

C_n^2 ($\text{m}^{-2/3}$)	ρ_0 (cm)	σ_χ^2
5×10^{-15}	6.8	0.01
5×10^{-14}	1.7	0.1

Table 1: Spherical-wave coherence length (ρ_0 and weak-perturbation spherical-wave logamplitude variance (σ_χ^2) versus turbulence strength (C_n^2) for a 1-km-long path at $1.55\,\mu\text{m}$ wavelength.

4.1. Focused-Beam Modes

The focused-beam mode set we will consider consists of the following $M = 225$ spatial patterns:

$$\Phi_{n_x,n_y}^{(0)}(\boldsymbol{\rho}) = \frac{\exp[-ik(x^2+y^2)/2L + i2\pi(n_x x + n_y y)/d]}{d}, \text{ for } -7 \le n_x, n_y \le 7, \tag{50}$$

for $\boldsymbol{\rho} \in \mathcal{A}_T$, where $\boldsymbol{\rho} = (x, y)$ in Cartesian coordinates. These modes are orthonormal on $\mathcal{A}_T$ in the $z = 0$ plane, focused on the $z = L$ plane, and have phase tilts—indexed by n_x and n_y—such that their orthogonality is very nearly preserved, for vacuum propagation, because $D_f = 400$. It is these vacuum-propagation $z = L$ patterns that our non-adaptive receiver will extract,

$$\phi_{n_x n_y}^{(0)}(\boldsymbol{\rho}') = \frac{\sqrt{D_f}}{d}\, e^{ik(x'^2+y'^2)/2L}\, \frac{\sin[\pi(\sqrt{D_f}x'/d - n_x)]}{\pi(\sqrt{D_f}x'/d - n_x)}\, \frac{\sin[\pi(\sqrt{D_f}y'/d - n_y)]}{\pi(\sqrt{D_f}y'/d - n_y)}, \text{ for } -7 \le n_x, n_y \le 7, \tag{51}$$

for $\boldsymbol{\rho}' \in \mathcal{A}_R$, where $\boldsymbol{\rho}' = (x', y')$ in Cartesian coordinates.

In Fig. 3(a) we have plotted the $\{\gamma_m^{\rm ad}\}$ and the $\{\kappa_m^{\rm non}\}$ versus m for our mild and moderate turbulence cases.[§] Also included is a plot of $\{\gamma_m^{\rm ad}\}$ for vacuum propagation (no turbulence), which lies almost directly under the $\{\gamma_m^{\rm ad}\}$ plot for mild turbulence. It is instructive to compare the values of $\sum_{m=1}^{225}\gamma_m^{\rm ad}$ and $\sum_{m=1}^{225}\kappa_m^{\rm non}$ with their ultimate—unity modal-transmissivity limit—of 225. This comparison is shown in Table 2, where we see that relatively little degradation has occurred, even in moderate turbulence, when ideal adaptive optics are employed. Consequently, as shown in Fig. 3(b), the ergodic Holevo capacities of the adaptive-optics system in both mild and moderate turbulence have lower bounds that are nearly coincident with the corresponding result for vacuum propagation, and, in fact, quite close to the upper bound. Moreover, the lower bounds for operation without adaptive optics—while implying that appreciable performance loss may occur, in these systems, when they are compared to the adaptive optics case—still indicate that high photon information efficiency *and* high spectral efficiency can be obtained. It should be noted, however, that there *will* be appreciable crosstalk between the spatial patterns generated in the receiver pupil $\mathcal{A}_R$ from transmission of the M FB modes we are considering.[28] The receiver that extracts the fixed mode patterns $\{\phi_{n_xn_y}^{(0)}(\boldsymbol{\rho}')\}$ will need to deal with this crosstalk to achieve the ergodic Holevo capacities whose lower bounds we have plotted in Fig. 3(b).

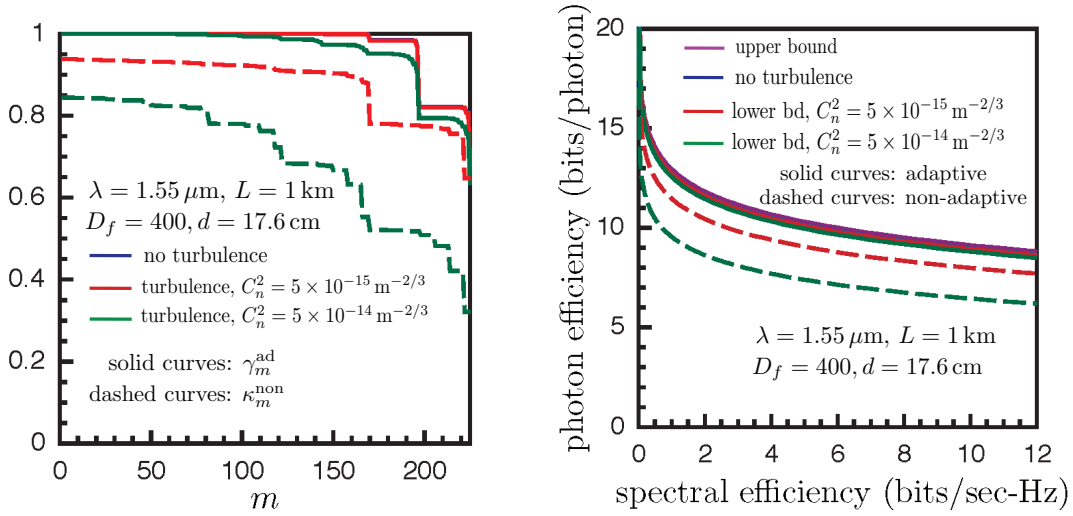

(a) FB-mode transmissivities

(b) FB-mode PIE vs/ SE bounds

Figure 3: Performance characteristics for an $M = 225$ FB-mode systems that do or do not use adaptive optics.

C_n^2 ($\mathrm{m}^{-2/3}$)	$\sum_{m=1}^{225}\gamma_m^{\rm ad}$	$\sum_{m=1}^{225}\kappa_m^{\rm non}$
0	219.15	214.33
5×10^{-15}	219.11	198.43
5×10^{-14}	215.86	156.96

Table 2: Comparison between FB-mode $\sum_{m=1}^{225}\gamma_m^{\rm ad}$ and $\sum_{m=1}^{225}\kappa_m^{\rm non}$; the maximum value for both of these quantities is 225.

[§]We are plotting versus a single mode-index m by arranging the $\{n_x, n_y\}$-indexed transmissivities in nonincreasing order. Similar single-argument indexing will be done in the next subsection for the transmissivities of the HG and LG modes.

4.2. Hermite-Gaussian and Laguerre-Gaussian Modes

The Hermite-Gaussian mode set we will consider consists of the following $M = 231$ spatial patterns:

$$\Phi^{(0)}_{n_x,n_y}(\boldsymbol{\rho}) = \frac{\sqrt{2\pi}(D_f)^{1/4}}{d\sqrt{\pi\, n_x!\, n_y!\, 2^{n_x+n_y}}}\, H_{n_x}\left(\frac{\sqrt{2\pi}(D_f)^{1/4}}{d}x\right) H_{n_y}\left(\frac{\sqrt{2\pi}(D_f)^{1/4}}{d}y\right) \exp\left[-\left(\frac{\pi\sqrt{D_f}}{d^2}+i\frac{k}{2L}\right)(x^2+y^2)\right], \quad (52)$$

for $\boldsymbol{\rho} \in \mathcal{A}_T$ and $1 \le n_x + n_y \le 21$, where $H_n(\cdot)$ is the nth Hermite polynomial. Strictly speaking, these modes are orthonormal on the infinite plane. For $D_f = 400$, however, they are very nearly orthonormal on $\mathcal{A}_T$. Furthermore, in vacuum propagation from $\mathcal{A}_T$ in the $z = 0$ plane to $\mathcal{A}_R$ in the $z = L$ plane, orthonormality is very nearly preserved, so that our non-adaptive receiver can use the vacuum-propagation output modes

$$\phi^{(0)}_{n_x,n_y}(\boldsymbol{\rho}') = \frac{\sqrt{2\pi}(D_f)^{1/4}}{d\sqrt{\pi\, n_x!\, n_y!\, 2^{n_x+n_y}}}\, H_{n_x}\left(\frac{\sqrt{2\pi}(D_f)^{1/4}}{d}x'\right) H_{n_y}\left(\frac{\sqrt{2\pi}(D_f)^{1/4}}{d}y'\right) \exp\left[-\left(\frac{\pi\sqrt{D_f}}{d^2}-i\frac{k}{2L}\right)(x'^2+y'^2)\right], \quad (53)$$

for $\boldsymbol{\rho}' \in \mathcal{A}_R$ and $1 \le 2p + |\ell| + 1 \le 21$.

The Laguerre-Gaussian mode set we will consider consists of the following $M = 231$ spatial patterns:

$$\Phi^{(0)}_{p,\ell}(\boldsymbol{\rho}) = \sqrt{\frac{p!}{\pi(|\ell|+p)!}}\frac{\sqrt{2\pi}(D_f)^{1/4}}{d}\left[\frac{\sqrt{2\pi}(D_f)^{1/4}}{d}\, r\right]^{|\ell|} L_p^{|\ell|}\left(\frac{2\pi\sqrt{D_f}}{d^2}\, r^2\right) \exp\left[-\left(\frac{\pi\sqrt{D_f}}{d^2}+i\frac{k}{2L}\right)r^2 + i\ell\theta\right], \quad (54)$$

for $\boldsymbol{\rho} \in \mathcal{A}_T$ and $1 \le n_x + n_y \le 21$, where $Lp^{\ell}(\cdot)$ is the generalized Laguerre polynomial, and $\boldsymbol{\rho} = (r, \theta)$ in polar coordinates. As was the case for our HG modes, these LG modes are orthonormal on the infinite plane. For $D_f = 400$, however, they are very nearly orthonormal on $\mathcal{A}_T$, and for vacuum propagation from $\mathcal{A}_T$ in the $z = 0$ plane to $\mathcal{A}_R$ in the $z = L$ plane this orthonormality is very nearly preserved. Hence our non-adaptive receiver for the LG modes can use the vacuum-propagation output modes

$$\phi^{(0)}_{p,\ell}(\boldsymbol{\rho}) = \sqrt{\frac{p!}{\pi(|\ell|+p)!}}\frac{\sqrt{2\pi}(D_f)^{1/4}}{d}\left[\frac{\sqrt{2\pi}(D_f)^{1/4}}{d}\, r'\right]^{|\ell|} L_p^{|\ell|}\left(\frac{2\pi\sqrt{D_f}}{d^2}\, r'^2\right) \exp\left[-\left(\frac{\pi\sqrt{D_f}}{d^2}-i\frac{k}{2L}\right)r'^2 + i\ell\theta'\right], \quad (55)$$

for $\boldsymbol{\rho}' \in \mathcal{A}_R$ and $1 \le 2p + |\ell| + 1 \le 21$, where $\boldsymbol{\rho}' = (r', \theta')$ in polar coordinates.

We are combining our discussions of the HG and LG modes for the following reason. For vacuum propagation between the infinite $z = 0$ and $z = L$ planes, for which the HG and LG modes are exact eigenfunctions, these mode sets are related by a unitary transformation. In particular the HG modes with $n_x + n_y + 1 = q$ are unitarily related to the LG modes with $2p + |\ell| + 1 = q$. Let $\mathbf{HGin}_q(\boldsymbol{\rho})$ denote the column vector of HG input modes with $n_x + n_y + 1 = q$ and $\mathbf{LG}^{\rm in}_q(\boldsymbol{\rho})$ denote the column vector LG input modes with $2p + |\ell| + 1 = q$. There is then a unitary matrix $\mathbf{U}_q$ such that

$$\mathbf{LG}^{\rm in}_q(\boldsymbol{\rho}) = \mathbf{U}_q\, \mathbf{HG}^{\rm in}_q(\boldsymbol{\rho}) \text{ and } \mathbf{HG}^{\rm in}_q(\boldsymbol{\rho}) = \mathbf{U}^{\dagger}_q\, \mathbf{LG}^{\rm in}_q(\boldsymbol{\rho}), \quad (56)$$

and the *same* $\mathbf{U}_q$ relates the column vector $\mathbf{HG}^{\rm out}_q(\boldsymbol{\rho}')$ of HG output modes with $n_x + n_y + 1 = q$ to the column vector $\mathbf{LG}^{\rm out}_q(\boldsymbol{\rho}')$ of LG output modes with $2p + |\ell| + 1 = q$. From these unitary transformations it is readily shown that the instantaneous power-transfer eigenvalues, $\{\mu^{\rm ad}_m\}$ and $\{\mu^{\rm non}_m\}$, for HG-mode operation with $1 \le n_x + n_y + 1 \le Q$ and LG-mode operation with $1 \le 2p + |\ell| + 1 \le Q$ are *identical*. This means that the ergodic Holevo capacities achieved with these mode sets coincide in propagation through atmospheric turbulence,

just as was found earlier for their vacuum-propagation Holevo capacities. Ensemble averaging does not break the unitary relationship. Hence the $\{\langle\mu_m^{\rm ad}\rangle\}$ and the $\{\langle\mu_m^{\rm non}\rangle\}$ are the same for the HG and LG mode sets with $1 \le n_x + n_y + 1 \le Q$ and $1 \le 2p + |\ell| + 1 \le Q$, respectively, and the same is true for their $\{\gamma_m^{\rm ad}\}$ and $\{\kappa_m^{\rm non}\}$. Thus, because the HG and LG mode sets we are considering here correspond to the $Q = 21$ case of this unitary equivalence, we have only calculated the HG-mode transmissivities and ergodic Holevo capacity bounds, because those calculations also apply to LG-mode operation.

In Fig. 4(a) we have plotted the $\{\gamma_m^{\rm ad}\}$ and the $\{\kappa_m^{\rm non}\}$ versus m for our mild and moderate turbulence cases. Also included is a plot of $\{\gamma_m^{\rm ad}\}$ for vacuum propagation (no turbulence), which lies almost directly under the $\{\gamma_m^{\rm ad}\}$ plot for mild turbulence. Once again it is instructive to compare the eigenvalue sums with their ultimate, unity modal-transmissivity, limit. This comparison is shown in Table 3, where we see that relatively little degradation has occurred, even in moderate turbulence, when ideal adaptive optics are employed. Consequently, as found for the FB modes, the ergodic Holevo capacities of the adaptive-optics system in both mild and moderate turbulence have lower bounds that are nearly coincident with the corresponding result for vacuum propagation, and, in fact, quite close to the upper bound; see Fig. 4(b). Also, the lower bounds for operation without adaptive optics—which show that appreciable performance loss may occur, in these systems, when they are compared to the adaptive optics case—still indicate that high photon information efficiency *and* high spectral efficiency can be obtained. This too was something seen earlier for the FB modes, as is the recognition that HG-mode or LG-mode receivers that extract fixed mode patterns will need to deal with substantial amounts of crosstalk[28] to achieve the ergodic Holevo capacities whose lower bounds we have plotted in Fig. 4(b). Interestingly, when we compare Figs. 3 and 4 we see that the focused-beam modes outperform the Hermite-Gaussian and Laguerre-Gaussian modes both when adaptive optics are employed and when they are not.

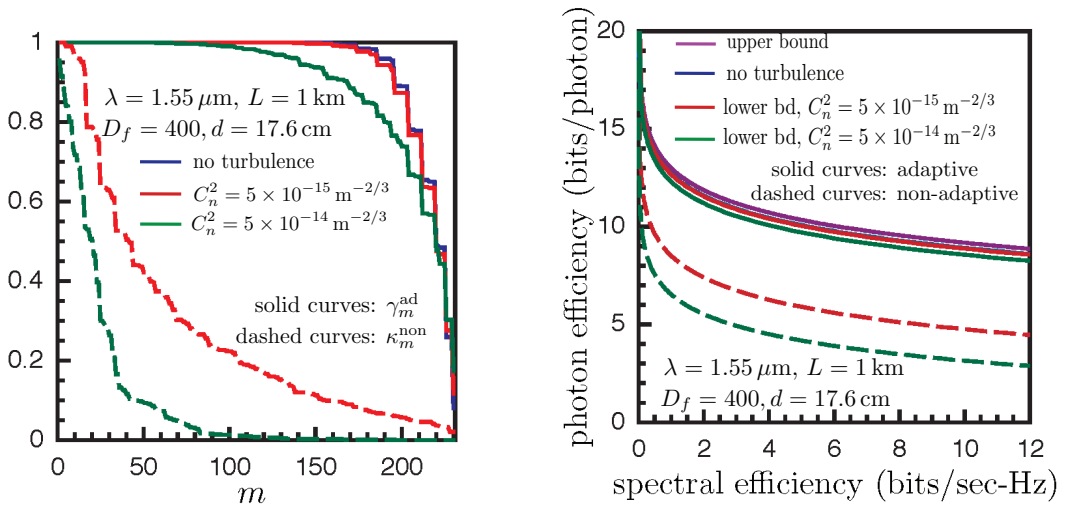

(a) HG-mode and LG-mode transmissivities

(b) HG-mode and LG-mode PIE vs. SE bounds

Figure 4: Performance characteristics for an $M = 231$ HG-mode and LG-mode systems that do or do not use adaptive optics.

C_n^2 (m$^{-2/3}$)	$\sum_{m=1}^{231} \gamma_m^{\rm ad}$	$\sum_{m=1}^{231} \kappa_m^{\rm non}$
0	216.96	195.76
5×10^{-15}	216.26	63.98
5×10^{-14}	207.49	22.93

Table 3: Comparison between $\sum_{m=1}^{231} \gamma_m^{\rm ad}$ and $\sum_{m=1}^{231} \kappa_m^{\rm non}$; the maximum value for both of these quantities is 231. The results shown apply to both the HG and the LG modes.

5. CONCLUSIONS

Driven by the desire to simultaneously realize high photon efficiency (many bits/detected photon) and high spectral efficiency (many bits/sec-Hz) in optical communication over a line-of-sight path through the turbulent atmosphere, we have developed results for the power-transfer transmissivities and the ergodic Holevo capacity when the transmitter uses a fixed set of M spatial modes and the receiver either does or does not employ adaptive optics. We were able to derive near-field transmissivity statistics that only require knowledge of the atmospheric Green's function's mutual coherence function *and* showed that they were sufficient to determine lower bounds for ergodic Holevo capacities of adaptive and non-adaptive operation. Sample calculations done for ∼200-mode communication over a 1 km path length at 1.55 μm wavelength with a square-pupil geometry whose vacuum-propagation Fresnel number product was 400 demonstrate that with perfect (full-wave) adaptive optics there is virtually no degradation from vacuum performance in photon information efficiency versus spectral efficiency behavior when the turbulence strength is mild. Furthermore, high photon efficiency plus high spectral efficiency is still possible when the turbulence strength is moderate, although here there is an appreciable performance reduction from what can be realized in vacuum. The preceding performance results were obtained for three transmitter mode sets: focused-beam modes, Hermite-Gaussian modes, and Laguerre-Gaussian modes. The latter two were shown, by virtue of their being related by a unitary transformation, to have identical modal-transmissivity spectra and ergodic Holevo capacities in the presence of turbulence, thus generalizing a result previously obtained for vacuum propagation. It turned out, however, that the FB modes outperformed the HG and LG modes for operation with and without adaptive optics, so, other things being equal, they might be the preferred choice.

There are several important avenues to pursue as follow-ons to the current work. First, a photon budget should be established for the adaptive-optics system's mode tracker: the PIE versus SE results we have presented presumed that perfect full-wave tracking was performed *and* that no accounting was made for the photons needed to accomplish that tracking. In addition, practical systems will very likely do only phase compensation, so this too should be considered in the future. Our results have been limited to ergodic Holevo capacities, for which capacity-achieving receiver implementations need to be found. While awaiting developments on that front, similar ergodic capacity bounds could be developed for the practical case of direct detection with OOK or PPM modulation.

6. ACKNOWLEDGMENTS

The research reported here was supported by the National Science Foundation IGERT program Interdisciplinary Quantum Information Science and Engineering (iQuISE), and by the DARPA Information in a Photon (InPho) program under DARPA/CMO Contract No. HR0011-10-C-1059.

REFERENCES

1. Boroson, D.M., Robinson, B.S., Burianek, D.Z. Murphy, D.V., and Biswas, A., "Overview and status of the Lunar Laser Communications Demonstration," Proc. SPIE **8246**, art. 82460C (2012).
2. Robinson, B.S., Kerman, A.J., Dauler, E.A., Barron, R.O., Caplan, D.O., Stevens, M.L., Carney, J.J., Hamilton, S.A., Yang, J.K.W., and Berggren, K.K., "781 Mbit/s photon-counting optical communications using a superconducting nanowire detector," Opt. Lett. **31**, pp. 444–446 (2006).
3. Essiambre, R.J., and Tkach, R.W., "Capacity trends and limits of optical communication networks," Proc. IEEE **100**, pp. 1035–1055 (2012).
4. Li, G., "Recent advances in coherent optical communication," Adv. Opt. Photon. **1**, pp. 279–307 (2009).
5. Guha, S., Dutton, Z., and Shapiro, J.H., "On quantum limit of optical communications: concatenated codes and joint detection receivers," Digest of the 2011 IEEE Internat. Sympos. on Inform. Theory, pp. 274–278 (IEEE, 2011).
6. Giovannetti, V., Guha, S., Lloyd, S., Maccone, L., Shapiro, J.H., and Yuen, H.P., "Classical capacity of the lossy bosonic channel: The exact solution," Phys. Rev. Lett. **92**, art. 027902 (2004).

7. Wilde, M.M., Guha, S., Tan, S.-H., and Lloyd, S., "Explicit capacity-achieving receivers for optical communication and quantum reading," Digest of the 2012 IEEE Internat. Sympos. on Inform. Theory, pp. 556–560 (IEEE, 2012).
8. Dolinar, S., Erkmen, B.I., Moision, B., Birnbaum, K., and Divsalar, D., "The ultimate limits of optical communication efficiency with photon-counting receivers," Digest of the 2012 IEEE Internat. Sympos. on Inform. Theory, pp. 546–550 (IEEE, 2012).
9. Slepian, D., "Analytical solution to two apodization problems," J. Opt. Soc. Am. **55**, pp. 1110–1114 (1965).
10. Healey, D.J.T., Wisely, D.R., Neild, I., and Cochrane, P. "Optical wireless: The story so far," IEEE Commun. Mag. **36**, 12, pp. 72–74 (Dec. 1998).
11. Kedar, D., and Arnon, S., "Urban optical wireless communication networks: The main challenges and possible solutions," IEEE Commun. Mag. **42**, 5, pp. S2–S7 (May 2004).
12. Kennedy, R.S., "Communication through optical scattering channels: An introduction," Proc. IEEE **58**, pp. 1651–1665 (1970).
13. Shapiro, J. H., "Imaging and optical communication through atmospheric turbulence," Chap. 6 in *Laser Beam Propagation in the Atmosphere*, J. W. Strohbehn, ed. (Springer-Verlag, 1978).
14. Shapiro, J.H., "Normal-mode approach to wave propagation in the turbulent atmosphere," Appl. Opt. **13**, pp. 2614–2619 (1974).
15. Erkmen, B.I., and Shapiro, J.H., "Performance analysis for near-field atmospheric optical communications," Proc. Globecom '04: IEEE Global Telecommun. Conf., pp. 318–324 (IEEE, 2004).
16. Shapiro, J.H., "Near-field turbulence effects on quantum key distribution," Phys. Rev. A **67**, art. 022309 (2003).
17. Shapiro, J.H., Guha, S., and Erkmen, B.I., "Ultimate channel capacity of free-space optical communications," J. Opt. Netw. **4**, pp. 501–515 (2005).
18. Saleh, A.A.M., "An investigation of laser wave depolarization due to atmospheric transmission," IEEE J. Quantum Electron. **3**, pp. 540–543 (1967).
19. Rushforth, C., and Harris, R., "Restoration, resolution, and noise," J. Opt. Soc. Am. **58**, pp. 539–544 (1968).
20. Toraldo di Francia, G., "Degrees of freedom of an image," J. Opt. Soc. Am. **59**, pp. 799–803 (1969).
21. Slepian, D. "Prolate spheroidal wave functions, Fourier analysis and uncertainty–IV: Extensions to many dimensions; generalized prolate spheroidal functions," Bell Syst. Tech. J., **43**, pp. 3009-3057 (1964).
22. Ishimaru, A., *Wave Propagation and Scattering in Random Media, Vol. 2* (Academic Press, 1978).
23. Andrews, L.C, and Phillips, R.L., *Laser Beam Scintillation with Applications* (SPIE, 2001).
24. Andrews, L.C., and Phillips, R.L., *Laser Beam Propagation through Random Media, Second Edition* (SPIE, 2005).
25. Paterson, C., "Atmospheric turbulence and orbital angular momentum of single photons for optical communication," Phys. Rev. Lett. **94**, art. 153901 (2005).
26. Anguita, J.A., Neifeld, M.A., and Vasic, B.V., "Turbulence-induced channel crosstalk in an orbital angular momentum-multiplexed free-space link," Appl. Opt. **47**, pp. 2414–2429 (2008).
27. Malik, M., O'Sullivan, M.O., Rodenburg, B., Mirhosseini, M. Leach, J. Lavery, M.P.J., Padgett, M.J., and Boyd, R.W., "Influence of atmospheric turbulence on optical communications using orbital angular momentum for encoding," Opt. Express **20**, pp. 13195–13200 (2012).
28. Chandrasekaran, N., and Shapiro, J.H., "Turbulence-induced crosstalk in multiple-spatial-mode optical communication," Digest of CLEO 2012, paper CF31.6 (Optical Society of American, 2012).